Excitons, biexcitons, and trions in self-assembled (In,Ga)As/GaAs quantum dots: Recombination energies, polarization, and radiative lifetimes versus dot height

Gustavo A. Narvaez, Gabriel Bester, and Alex Zunger
National Renewable Energy Laboratory, Golden, Colorado 80401, USA
(Received 1 September 2005; published 13 December 2005)

We calculate the height dependence of recombination energies, polarization, and radiative lifetimes of the optical transitions of various excitonic complexes: neutral excitons (X^0), negatively (X^-) and positively charged (X^+) trions, and biexcitons (XX^0) in lens-shaped, self-assembled $In_{0.6}Ga_{0.4}As/GaAs$ quantum dots. By using an atomistic pseudopotential method combined with the configuration-interaction method, we predict the following. (i) The recombination energy of the lowest transition of X^- blueshifts as height increases, whereas that of X^+ redshifts. Remarkably, the recombination of XX^0 shows a redshift at small heights, reaches a maximum shift, and then blueshifts for taller dots. This feature results from the height dependence and relative magnitude of the interelectronic direct Coulomb interaction. (ii) Changes in dot height lead to a bound-to-unbound crossover for X^-, X^+, and XX^0. (iii) When considering the [110] and $[1\bar{1}0]$ directions, the lowest transitions of X^0 and XX^0 manifest [110] vs $[1\bar{1}0]$ in-plane polarization anisotropy that switches sign as a function of height as well as alloy randomness. X^- and X^+ show transitions with negligible polarization anisotropy regardless of height. (iv) The ground state of X^0 is split in a low-energy pair that is forbidden (dark) and a high-energy pair that is allowed; thus, at $T=0$ K, the radiative lifetime $\tau(X^0)$ is long ($\sim$ ms) due to the dark exciton. On the other hand, at $T=10$ K, $\tau(X^0)$ decreases moderately as height increases and its magnitude ranges from 2–3 ns. The ground state of X^- and X^+, and that of XX^0 is allowed (bright); so, $\tau(X^-)$, $\tau(X^+)$, and $\tau(XX^0)$ are fast ($\sim$ ns) even at $T=0$ K. These radiative lifetimes depend weakly on height. In addition, $\tau(X^-) \sim \tau(X^+) \simeq 1.1$ ns, while $\tau(XX^0) \simeq 0.5$ ns. We compare our predictions with available spectroscopic data.

DOI: 10.1103/PhysRevB.72.245318 PACS number(s): 71.35.Pq, 73.21.La

I. INTRODUCTION

Single-dot spectroscopy makes it possible to probe dot-to-dot changes in the excitonic properties of self-assembled $In_xGa_{1-x}As/GaAs$ quantum dots.[1–9] Both single-particle and many-particle aspects of these properties depend nontrivially on the quantum dots size and shape,[10] reflecting not only simple quantum-confinement physics, but also electronic structure effects such as interband, intervalley, spin-orbit and strain-induced state coupling. The description of these effects requires an atomistic multiband approach.[11–15] Here we adopt a method that is based on screened pseudopotentials and the configuration-interaction approach, and address the changes with height of recombination (emission) energies, polarization and radiative lifetimes of various neutral and charged excitons: the neutral exciton (X^0), negatively (X^-) and positively charged (X^+) excitons, and the biexciton (XX^0) in lens-shaped, self-assembled alloyed $In_{0.6}Ga_{0.4}As/GaAs$ quantum dots. Our predictions compare reasonably well with available spectroscopic data. We also compare our findings in $In_{0.6}Ga_{0.4}As/GaAs$ dots with those in pure, nonalloyed InAs/GaAs dots.

II. ENERGETICS OF THE MONOEXCITON, CHARGED TRIONS, AND BIEXCITON

A. Electronic structure of the excitonic manifolds

We describe the basic electronic structure of the excitonic manifolds (Fig. 1) before describing recombination processes. All excitonic states are based on mixing and excitations of the single-particle states $\{h_0, h_1, h_2, \ldots\}$ and $\{e_0, e_1, e_2, \ldots\}$, for holes and electrons, respectively. These states are solutions of the single-particle Schrödinger equation

$$\left\{-\frac{1}{2}\nabla^2 + V_{ext}(\mathbf{R}) + V_{scr}(\mathbf{R})\right\}\psi_i = \mathcal{E}_i\psi_i, \tag{1}$$

where both the external (pseudo) potential $V_{ext}(\mathbf{R})$ due to the ion-ion and ion-electron interaction and the screening response to such external potential $V_{scr}(\mathbf{R})$ are expressed as a superposition of screened atomic pseudopotentials

$$V_{ext}(\mathbf{R}) + V_{scr}(\mathbf{R}) = V_{SO} + \sum_l \sum_\alpha v_\alpha[\mathbf{R} - \mathbf{R}_l^{(\alpha)}; \mathrm{Tr}(\tilde{\varepsilon})]. \tag{2}$$

Here, V_{SO} is a nonlocal spin-orbit interaction;[16] v_α is a screened pseudopotential for atom of type α that depends on strain, and it has been fitted to *bulk* properties of GaAs and InAs, including bulk band structures, experimental deformation potentials and effective masses, as well as local-density-approximation (LDA)-determined band offsets.[16] The single-particle Shrödinger equation [Eq. (1)] includes not only quantum-confinement effects (as in simple, one-band particle-in-a-box models), but also multi-band coupling (light hole, heavy hole, conduction); intervalley (Γ-X-L) coupling; and spin-orbit coupling. Strain effects are present through the relaxation, via a valence force field,[16] of the atomic positions $\{\mathbf{R}_l^{(\alpha)}\}$ within the simulation supercell (quantum dot+GaAs-matrix); and directly "felt" by the potential $v_\alpha[\mathbf{R}-\mathbf{R}_l^{(\alpha)}; \mathrm{Tr}(\tilde{\varepsilon})]$. States $\{h_0, h_1, h_2, \ldots\}$ and

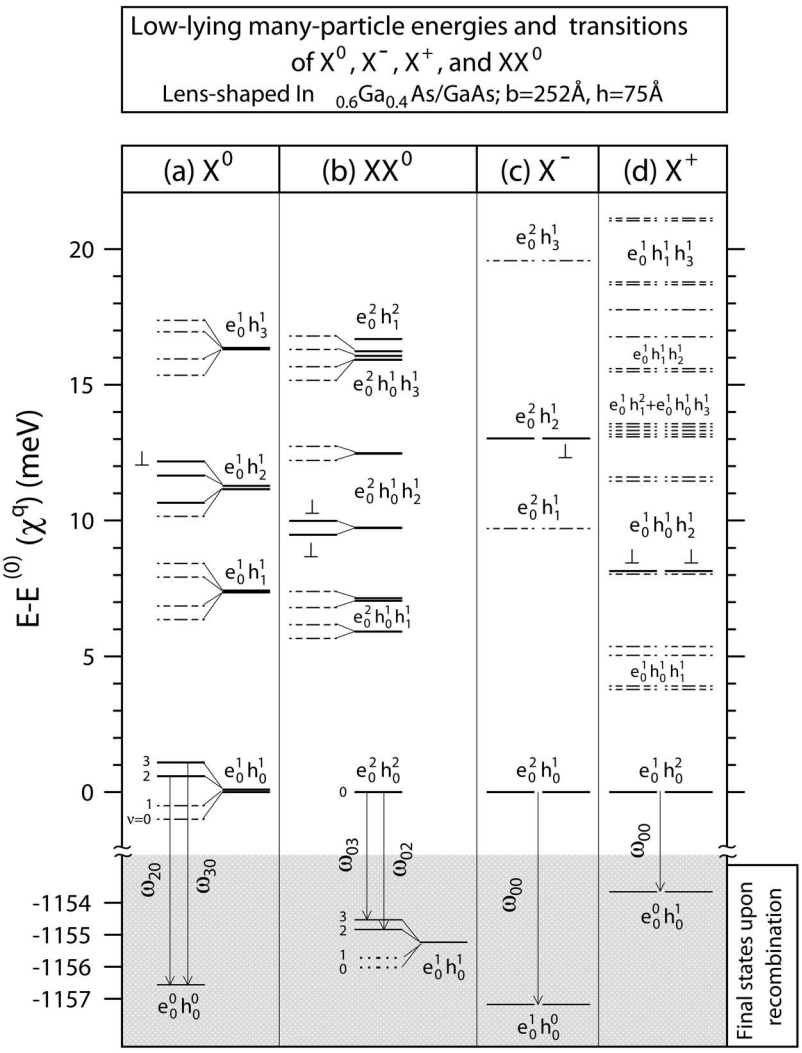

FIG. 1. Quantitative many-particle, configuration-interaction low-lying energies and lowest optical transitions for (a) X^0, (b) XX^0, (c) X^-, and (d) X^+ in a lens-shaped $In_{0.6}Ga_{0.4}As/GaAs$ dot with base diameter $b=252$ Å and height $h=75$ Å. In each panel, the energy is shown relative to the ground-state energy of the corresponding exciton χ^q (=X^0, X^-, X^+, and XX^0). Two horizontally aligned dashes and dotted lines indicate, respectively, twofold degenerate bright and dark levels. The dominant single-particle configuration of each excitonic level is indicated by $e_0^p h_j^q h_{j'}^{q'}$, where p, q, and $q'(=0,1,2)$ indicate, correspondingly, the occupation of the electron level e_0 and hole levels h_j and $h_{j'}$. The energy of allowed transitions (vertical arrows) is indicated by ω_{if}, where i and f indicate, respectively, the initial and final state upon recombination. Bright and dark excitonic levels are indicated, respectively, by solid and dotted lines. The fine-structure splittings are shown schematically.

$\{e_0, e_1, e_2, \ldots\}$ form a basis for the excitonic states. We indicate the dominant single-particle configuration of each excitonic level by $e_i^p e_{i'}^{p'} h_j^q h_{j'}^{q'}$, where p, p', q, and q' $(=0,1,2)$ indicate, correspondingly, the occupation of the electron levels e_i and $e_{i'}$, and hole levels h_j and $h_{j'}$. Figure 1 illustrates the excitonic manifolds using a 75 Å-tall lens-shaped $In_{0.6}Ga_{0.4}As/GaAs$ quantum dot (base diameter $b=252$ Å), as obtained from configuration-interaction calculations based on the pseudopotential single-particle description.

Monoexciton. The monoexciton X^0 has a ground-state $|\Psi^{(0)}(X^0)\rangle$ created by occupying h_0 and e_0, denoted $e_0^1 h_0^1$ [Fig. 1(a)]. However, configuration-interaction[17] (CI) also mixes into $|\Psi^{(0)}(X^0)\rangle$ other states such as $e_0^1 h_1^1, e_0^1 h_2^1, \ldots$. This is done by expanding the monoexciton states $\{|\Psi^{(\nu)}(X^0)\rangle\}$ $(\nu=0,1,2,\ldots)$ in a basis of Slater determinants (configurations) $\{|\Phi(X^0)\rangle\}$ constructed in the subspace of N_e and M_h electron and hole confined single-particle levels, respectively,

$$|\Psi^{(\nu)}(X^0)\rangle = \sum_{\kappa} C_{\kappa}^{(\nu)}(X^0)|\Phi_{\kappa}(X^0)\rangle, \tag{3}$$

where $C_{\kappa}^{(\nu)}(X^0)$ are the CI coefficients and κ is a composite index that labels each Slater determinant. Since e_0 and h_0 are each twofold degenerate due to spin, $e_0^1 h_0^1$ has fourfold degeneracy at the single-particle level of Eqs. (1) and (2). We next allow Coulomb electron-electron and hole-hole interactions. Direct Coulomb is given by $J_{ij;ji}^{(\mu\mu)}$ and exchange by $J_{ij;ij}^{(\mu\mu)}$, with the Coulomb scattering matrix elements given by

$$J_{ij;kl}^{(\mu\mu')} = \int\int d\mathbf{R}d\mathbf{R}' \frac{[\psi_i^{(\mu)}(\mathbf{R})]^*[\psi_j^{(\mu')}(\mathbf{R}')]^*[\psi_k^{(\mu')}(\mathbf{R}')][\psi_l^{(\mu)}(\mathbf{R})]}{\epsilon(\mathbf{R},\mathbf{R}')|\mathbf{R}-\mathbf{R}'|}, \tag{4}$$

Here $\mu, \mu' = e, h$; and $\epsilon(\mathbf{R},\mathbf{R}')$ is a microscopic, phenomenological dielectric constant.[18] We also allow electron-hole direct Coulomb interaction $J_{ij;ji}^{(eh)}$ and electron-hole exchange

$$K_{ij;kl}^{(eh)} = \int\int d\mathbf{R}d\mathbf{R}' \frac{[\psi_i^{(h)}(\mathbf{R})]^*[\psi_j^{(e)}(\mathbf{R}')]^*[\psi_k^{(e)}(\mathbf{R})][\psi_l^{(h)}(\mathbf{R}')]}{\epsilon(\mathbf{R},\mathbf{R}')|\mathbf{R}-\mathbf{R}'|}. \tag{5}$$

Inclusion of these Coulomb interactions splits $e_0^1 h_0^1$ into four distinct levels:[19,20] The lowest two are spin-forbidden ("dark") in the absence of spin-orbit coupling, and the highest two are allowed ("bright"). The bright-dark splitting of

the ground-state levels shown in Fig. 1(a) is 84 μeV. The magnitude of this splitting increases up to 178 μeV for a 20 Å-tall dot. At $T\sim 0$ K only the dark states are populated, thus, the transition to the ground state $e_0^0h_0^0$ is long-lived. Figure 1(a) (shaded area) shows transitions ω_{20} and ω_{30} from the bright states to $e_0^0h_0^0$. The low-lying excited states of the monoexciton correspond to excitations of the hole, i.e., $e_0^1h_1^1$, $e_0^1h_2^1$ and $e_0^1h_3^1$, due to the much smaller spacing of hole single-particle energy levels compared to that of the electrons. Thus, the spacing of the excited states fingerprint the hole energy level structure. Figure 1(a) shows the first twelve excited states that are derived from $e_0^1h_1^1$, $e_0^1h_2^1$ and $e_0^1h_3^1$. Each of these states are four-fold degenerate and their fine structure is shown schematically. We find that three out of the four levels that arise from $e_0^1h_2^1$ are optically allowed. In particular, one of the levels, indicated as $\perp$, emits light that is polarized along [001], while the remaining two emit in-plane polarized light. These excited levels become optically forbidden as the dot becomes flatter.

Biexciton. In contrast to the four levels comprising the monoexciton, the biexciton XX^0 has a singly-degenerate, *closed-shell* ground state ($e_0^2h_0^2$) that is bright. Thus, even at $T\sim 0$ K both emissions ω_{03} and ω_{02} [Fig. 1(b); shaded area] of the biexciton are fast ($\sim$ ns). The biexciton has a nontrivial ladder of excited states that is determined primarily by the relative magnitude of the direct Coulomb hole-hole interaction and the single-particle energy splittings of the hole states. The ladder begins with states derived from $e_0^2h_0^1h_1^1$ at about 6 meV above the ground state and follows with $e_0^2h_0^1h_2^1$ and $e_0^2h_0^1h_3^1$ at about 11 meV and 16 meV, respectively. Due to the two-fold Kramers degeneracy of the hole levels, $e_0^2h_0^1h_1^1$ is four-fold degenerate at the single-particle level, these states split into four distinct states due to hole-hole and electron-hole exchange [Fig 1(b)]. Similarly, the four states in $e_0^2h_0^1h_2^1$ split in two groups of two. In this case, remarkably, the splitting is about twice as big as that in $e_0^2h_0^1h_1^1$ and nearly five times bigger than in $e_0^2h_0^1h_3^1$ ($\sim$500 μeV). Similarly to the monoexciton case, the lowest split-off pair in $e_0^2h_0^1h_2^1$ is optically active and emits light polarized along [001] [$\perp$, Fig. 1(b)]. Further, these states become darker as the dot becomes flatter, being forbidden at $h=20$ Å. The subsequent excited state in the ladder derives from the singly-degenerate closed-shell state $e_0^2h_1^2$ and is closely-spaced with $e_0^2h_0^1h_3^1$. Note that albeit the splitting between these states is small, the state derived from the closed-shell configuration $e_0^2h_1^2$ is relatively "inert" in that it mixes weakly with other states. In particular the weight of this configuration in the CI expansion is $\sim$83%. Below, we discuss the energy, polarization and lifetime of ω_{03} and ω_{02}.

Trions. The negatively (X^-) and positively charged (X^+) trions have ground states that are bright, two-fold degenerate and arise from occupying $e_0^2h_0^1$ and $e_0^1h_0^2$, respectively. Due to configuration-interaction mixing, the ground states of X^- and X^+ mix with $e_0^2h_1^1$ and $e_0^1h_0^1h_1^1$, respectively. As in the case of XX^0, even at $T\sim 0$ K the recombination ω_{00} of X^- [Fig. 1(c)] into state $e_0^1h_0^0$ and that of X^+ [Fig. 1(d)] into state $e_0^0h_0^1$ is fast. For both trions, while there are only two dipole-allowed transitions in the absence of spin-orbit coupling, we predict four allowed transitions. The first few excited states of X^- correspond to occupying states derived primarily from $e_0^2h_1^1$, $e_0^2h_2^1$ and $e_0^2h_3^1$ [Fig. 1(c)]. (Naturally, these states are mixed in with other states of X^-.) These excited states are two-fold degenerate and lie, correspondingly, about 10 meV, 13 meV and 20 meV above the ground state, as shown in Fig. 1(c). Note the similarity of the low-lying excited states energy spacing with that in X^0. In addition, note that one of the two states derived from $e_0^2h_2^1$ is optically active and emits light polarized along [001] [$\perp$ in Fig. 1(c)]. Again, these states become optically forbidden for a 20 Å-tall dot. The excited states of X^+ are more complex and present a high density of states [Fig. 1(d)]; a consequence of the closely spaced ($\sim$5 meV) single-particle hole levels: In contrast to X^-, all low-lying excited states show fine-structure splitting due to electron-hole exchange. The first excited states at about 5 meV corresponds to occupying $e_0^1h_0^1h_1^1$, due to the twofold degeneracy of each of these single-particle states, there are eight excited states that split in two groups of four, due to hole-hole exchange. Occupying $e_0^1h_0^1h_2^1$ leads to the next eight excited states around 10 meV, which are also split in two quartets. In this case, there is an optically active (polarization $\parallel$ [001]) pair of excited states that belong to the lower-energy quartet [$\perp$, Fig. 1(d)]. As in the other excitons, these states become dark as the dot height decreases. The next ten excited states about 14 meV are a mixture of eight configurations derived from $e_0^1h_0^1h_3^1$ and two from $e_0^1h_1^2$. Because e_0 is *half-filled*, $e_0^1h_1^2$ is very "reactive" in the sense that it heavily mixes via configuration interaction. Note that this is significantly different from the case of configuration $e_0^2h_0^2$ in the biexciton [Fig. 1(b)]. Higher excited states correspond to occupying $e_0^1h_1^1h_2^1$ and $e_0^1h_1^1h_3^1$. Below, we discuss the energy, as well as polarization and lifetime of ω_{00} for X^- and X^+.

B. Recombination energies

We define the recombination energy upon recombination of an electron-hole pair in χ^q as the difference between the total energies of the initial state $|\Psi^{(i)}(\chi^q)\rangle$ and the final state $|\Psi^{(f)}(\chi^q-1)\rangle$. Namely,

$$\omega_{i0}(X^0) = E^{(i)}(X^0),$$

$$\omega_{if}(X^-) = E^{(i)}(X^-) - \mathcal{E}_f^{(e)},$$

$$\omega_{if}(X^+) = E^{(i)}(X^+) + \mathcal{E}_f^{(h)},$$

$$\omega_{if}(XX^0) = E^{(i)}(XX^0) - E^{(f)}(X^0), \qquad (6)$$

where i and f label an initial and final state, respectively; $\mathcal{E}_f^{(e)}$ and $\mathcal{E}_f^{(h)}$ are, respectively, the single-particle energy of the electron and hole in the final state; and $E^{(\nu)}(\chi^q)$ is the multiparticle, configuration-interaction energy of state $|\Psi^{(\nu)}(\chi^q)\rangle$. [In Eq. (6), the energy of the ground state of the system in the absence of excited electron-hole pairs is taken to be zero.] Optical experiments like photoluminescence probe electron-hole recombination transitions that are

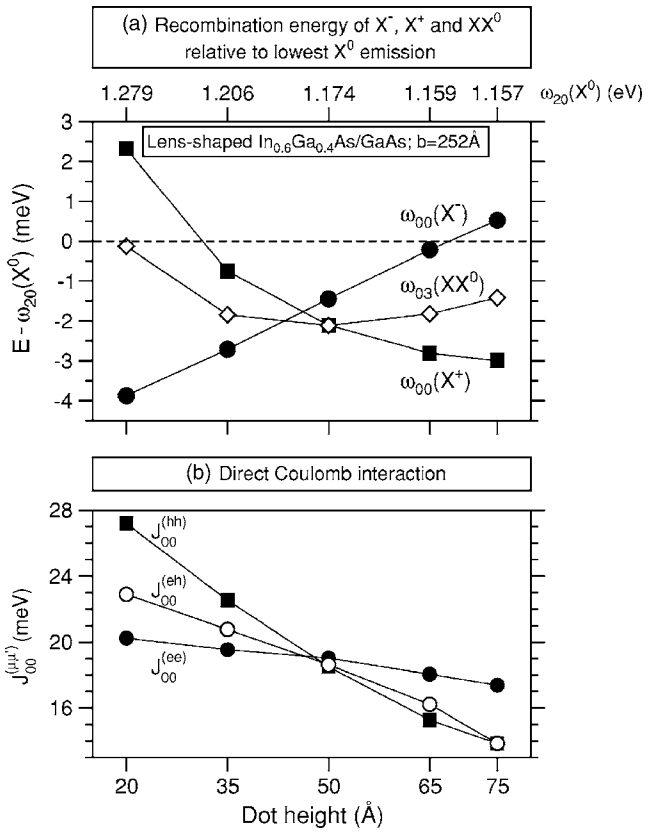

FIG. 2. (a) Recombination energies $\omega_{00}(X^-)$ and $\omega_{00}(X^+)$, and $\omega_{03}(XX^0)$ (see text and Fig. 1) in $In_{0.6}Ga_{0.4}As/GaAs$ quantum dots (base $b=252$ Å) with different heights. The energy is shown as a spectroscopic shift relative to $\omega_{20}(X^0)$ [see Fig. 1(a)]. (b) Screened direct Coulomb interaction $J_{00}^{(\mu\mu')}$ versus dot height. At $h=50$ Å a nearly "symmetric" regime $[J_{00}^{(eh)} \sim J_{00}^{(hh)} \sim J_{00}^{(ee)}]$ is attained.

allowed (bright).[21] Figures 1(a)–1(d) indicates with arrows thelowest bright recombination transitions of exciton χ^q, for a 75 Å tall lens-shaped $In_{0.6}Ga_{0.4}As/GaAs$ dot with base diameter $b=252$ Å. The final states upon electron-hole recombination are presented in the shaded area of Fig. 1. Figure 2 shows the recombination energies $\omega_{00}(X^-)$, $\omega_{00}(X^+)$ and $\omega_{03}(XX^0)$ calculated at the many-particle, configuration-interaction level as a function of dot height. These recombination energies are shown relative to the lowest recombination energy $\omega_{20}(X^0)$ of the monoexciton (the latter energy is shown in the top axis of Fig. 2). Thus, the results correspond to *spectroscopic shifts* that are currently measured by several groups. Prominent features are the following:

(i) The recombination energy $\omega_{00}(X^-)$ blue-shifts as height increases; in contrast, $\omega_{00}(X^+)$ red-shifts. These trends have been explained by Bester and Zunger in Ref. 22 by adopting the Hartree-Fock approximation.

(ii) For the flattest dot ($h=20$ Å) the ordering $\omega_{00}(X^+) > \omega_{20}(X^0) > \omega_{00}(X^-)$ of the emission energies and the relative magnitude of the spectroscopic shifts $\omega_{00}(X^+) - \omega_{20}(X^0) < \omega_{20}(X^0) - \omega_{00}(X^-)$ agree with photoluminescence (PL) data.[2–5] These relationships are explained at the Hartree-Fock level of approximation, as in Ref. 22, in which one derives

$$\omega_{20}(X^0) = [\mathcal{E}_0^{(e)} - \mathcal{E}_0^{(h)}] - J_{00}^{(eh)}, \tag{7}$$

$$\omega_{00}(X^+) = [\mathcal{E}_0^{(e)} - \mathcal{E}_0^{(h)}] + J_{00}^{(hh)} - 2J_{00}^{(eh)}, \tag{8}$$

$$\omega_{00}(X^-) = [\mathcal{E}_0^{(e)} - \mathcal{E}_0^{(h)}] + J_{00}^{(ee)} - 2J_{00}^{(eh)}. \tag{9}$$

Then, the relationship $J_{00}^{(hh)} > J_{00}^{(eh)} > J_{00}^{(ee)}$ that holds at $h=20$ Å [Fig. 2(b)] reveals the ordering of the emission energies and the magnitude of the spectroscopic shifts. Regarding the magnitude of the spectroscopic shifts, $\omega_{00}(X^+) - \omega_{20}(X^0) = 2.5$ meV and $\omega_{00}(X^-) - \omega_{20}(X^0) = -3.7$ meV agree reasonably well with (a) 2 meV and −6 meV, respectively, that Ware and co-workers have recently observed in an InAs/GaAs dot (size unspecified) with monoexciton emission at ~1.268 eV (Ref. 2); also with (b) $\omega_{00}(X^-) - \omega_{20}(X^0) = -5$ meV measured by Smith *et al.* in an $In_xGa_{1-x}As/GaAs$ dots (size unspecified) with emission energy at ~1.319 eV (Ref. 1); and with (c) the value of −5.8 meV for $\omega_{00}(X^-) - \omega_{20}(X^0)$ observed by Finley and co-workers in an $In_xGa_{1-x}As/GaAs$ dots $[b=(230\pm70)$ Å, $h=(25\pm10)$ Å] with emission at ~1.263 eV (Ref. 5).

(iii) As height increases, $\omega_{03}(XX^0)$ redshifts at small heights, reaches a maximum shift of nearly −2 meV at $h \sim 50$ Å, and then it moderately blueshifts for taller dots. In addition, at $h=50$ Å the emission energy of XX^0 coincideswith that of X^+. As in (ii), these results are explained at the Hartree-Fock level, which predicts

$$\omega_{03}(XX^0) - \omega_{20}(X^0) = J_{00}^{(ee)} + J_{00}^{(hh)} - 2J_{00}^{(eh)}, \tag{10}$$

$$\omega_{03}(XX^0) - \omega_{00}(X^+) = J_{00}^{(ee)} - J_{00}^{(eh)}. \tag{11}$$

Here, we have neglected the small (~1–6 μeV) splitting of the monoexciton bright states. Then, by analyzing the height dependence of the direct Coulomb interactions $J_{00}^{(ee)}$, $J_{00}^{(hh)}$ and $J_{00}^{(eh)}$ [Fig. 2(b)] we find that Eq. (10) predicts the observed height dependence of $\omega_{03}(XX^0)$, although the actual magnitude of the emission is not quantitatively predicted due to correlations.[23,24] In addition, Eq. (11) reveals the coincidence of the emission of XX^0 and that of X^+ as a result of balancing the magnitudes of $J_{00}^{(ee)}$ and $J_{00}^{(eh)}$ at $h=50$ Å. The latter balance arises from the similar degree of localization of $\psi_0^{(e)}$ and $\psi_0^{(h)}$ within the dot.[25]

(iv) $\omega_{03}(XX^0) - \omega_{20}(X^0) = -2.0$ meV at $h=50$ Å agrees with the value of -2.0 ± 0.1 meV for XX^0 measured by Finley and co-workers in PL experiments in an $In_xGa_{1-x}As/GaAs$ dot $[b=(230\pm70)$ Å and $h=(25\pm10)$ Å] with exciton ground-state emission at ~1.345 eV (Ref. 5). In addition, this result of −2.0 meV for the biexciton shift agrees remarkably well with the value of −2 meV measured by Rodt *et al.* in InAs/GaAs dots ($b=100-200$ Å, height unspecified) with monoexciton emission energies ranging between 1.260 eV and 1.295 eV (Ref. 6); and also with the measured shift of −2.3 meV observed by Urbaszek and co-workers in $In_xGa_{1-x}As/GaAs$ dots (size unspecified) with monoexciton emission energy of 1.294 eV (Ref. 7). The value of about −1.7 meV for $\omega_{03}(XX^0) - \omega_{20}(X^0)$ that we find at $h=35$ Å and 65 Å agrees well with the value of −1.6 meV observed by Bayer and co-workers in $In_xGa_{1-x}As/GaAs$ dots [b

$=(500\pm30)$ Å] with exciton emission at 1.428 eV (Ref. 26). Our results also agree satisfactorily with the value of −2.7 meV measured by Findeis and co-workers in dots (size unspecified) with monoexciton emission energy at 1.284 eV (Ref. 8).

C. Binding energies

The binding energies of excitons χ^q are defined as

$$\Delta(X^0) = [\mathcal{E}_0^{(e)} - \mathcal{E}_0^{(h)}] - E^{(0)}(X^0),$$

$$\Delta(X^-) = [\mathcal{E}_0^{(e)} + E^{(0)}(X^0)] - E^{(0)}(X^-),$$

$$\Delta(X^+) = [-\mathcal{E}_0^{(h)} + E^{(0)}(X^0)] - E^{(0)}(X^+),$$

$$\Delta(XX^0) = 2E^{(0)}(X^0) - E^{(0)}(XX^0). \quad (12)$$

Exciton χ^q is said to be *bound* when the binding energy $\Delta(\chi^q)$ is positive. Conversely, $\Delta(\chi^q)<0$ implies the exciton is unbound. Note that the binding energy is defined with respect to the ground-state energy of *dissociated* excitonic complexes. For instance, the binding energy of X^0 is defined with respect to the energy of a non-interacting electron-hole pair. In turn, the binding energy of the biexciton XX^0 is defined with respect to the total energy of two non-interacting monoexcitons [Eq. (12)].

Figure 3 shows $\Delta(X^0)$, $\Delta(X^-)$, $\Delta(X^+)$, and $\Delta(XX^0)$ as well as $E^{(0)}(X^0)$ as a function of dot height. $\Delta(X^0)$ decreases with increasing height, and it is well approximated by $J_{00}^{(eh)}$ as correlation effects are relatively small (~2 meV). The height dependence of the binding energy of X^-, X^+, and XX^0 follows the height dependence of the spectroscopic shifts shown in Fig. 2(a). This is so because the bright-dark splitting for the monoexciton X^0 is small ~80–180 μeV. As expected from the spectroscopic shifts results [Fig. 2(a)], the height dependence of the binding energy is qualitatively different for each exciton χ^q. (i) $\Delta(X^-)$ is bound (~4 meV) for the flattest dot ($h=20$ Å) and it decreases almost linearly, becoming unbound for dots taller than $h=65$ Å. (ii) In contrast, $\Delta(X^+)$ is unbound for the flattest dot and increases up to 3 meV, becoming bound slightly below $h=35$ Å. (iii) $\Delta(XX^0)$ does not depend monotonically on the gap, reaching a maximum around $h=50$ Å. In addition, XX^0 is bound [$\Delta(XX^0)>0$] for all heights above 20 Å while unbound for the flattest dot ($h=20$ Å). The latter is due to an interplay between Hartree-Fock and correlation contributions to binding, $\Delta_{\mathrm{HF}}(XX^0)$ and $\delta(XX^0)$, respectively, that results in correlation being insufficient to bind XX^0. Namely,

$$\begin{aligned}\Delta(XX^0) &= \Delta_{\mathrm{HF}}(XX^0) + \delta(XX^0)\\ &= \{2J_{00}^{(eh)} - [J_{00}^{(ee)} + J_{00}^{(hh)}]\} + \delta(XX^0)\\ &= -1.6\ \mathrm{meV} + 1.4\ \mathrm{meV}\\ &= -0.2\ \mathrm{meV}. \quad (13)\end{aligned}$$

It should be noted that Rodt and co-workers[6] observed (in photoluminescence) a bound-unbound crossover for XX^0 as the monoexciton emission energy of $In_xGa_{1-x}As/GaAs$ quantum dots decreased. Those authors also calculated the binding energy of XX^0, using an 8-band $\mathbf{k}\cdot\mathbf{p}$ model, and suggested that the reduction of correlation effects was responsible for unbinding XX^0 as the gap increased.[6]

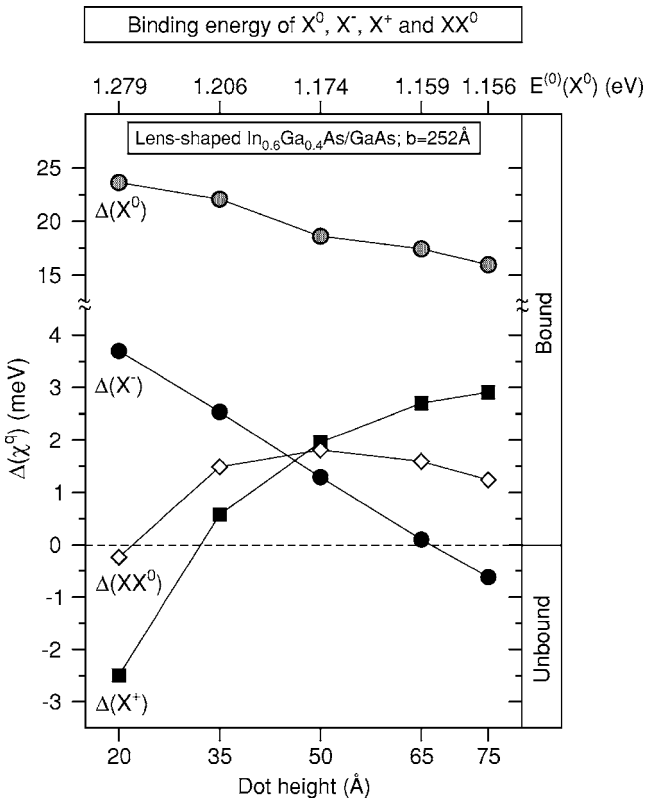

FIG. 3. Binding energy $\Delta(\chi^q)$ [Eq. (12)] of X^0, X^-, and X^+, and XX^0 as a function of dot height. The ground-state energy $E^{(0)}(X^0)$ of X^0 is also shown (top axis). For X^-, X^+, and XX^0, height drives a bound-to-unbound crossover.

III. POLARIZATION ANISOTROPY OF OPTICAL TRANSITIONS

When an electron-hole pair in exciton χ^q recombines optically, the transition is characterized by both the transition energy $\omega_{if}(\chi^q)$ [Eq. (6)] and the transition dipole matrix element

$$\mathrm{M}_{if}^{(\hat{\mathbf{e}})}(\chi^q) = \langle\Psi^{(f)}(\chi^q - 1)|\hat{\mathbf{e}}\cdot\mathbf{p}|\Psi^{(i)}(\chi^q)\rangle. \quad (14)$$

Here, $\mathbf{p}$ is the electron momentum and $\hat{\mathbf{e}}$ is the polarization vector of the electromagnetic field.[21]

The dipole matrix elements $\mathrm{M}_{if}^{(\hat{\mathbf{e}})}(\chi^q)$ [Eq. (14)] depend on the polarization vector $\hat{\mathbf{e}}$; so, it is natural to quantify what is the degree of polarization anisotropy between different polarizations $\hat{\mathbf{e}}_1$ and $\hat{\mathbf{e}}_2$. Therefore, we introduce the recombination (emission or pholuminescence) intensity spectrum of exciton χ^q for polarization $\hat{\mathbf{e}}$,

$$I^{(\hat{\mathbf{e}})}(\omega,T;\chi^q) = \sum_{i,f} |\mathrm{M}_{if}^{(\hat{\mathbf{e}})}(\chi^q)|^2 P_i(T;\chi^q)\,\delta[\omega - \omega_{if}(\chi^q)]. \quad (15)$$

Here,

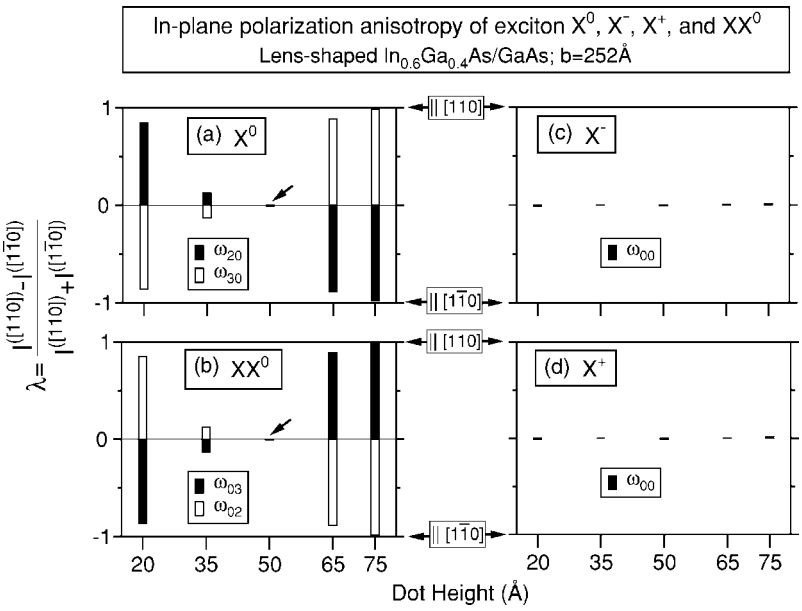

FIG. 4. In-plane polarization anistropy λ [Eq. (17)] for the lowest optical transitions of (a) X^0, (b) XX^0, (c) X^-, and (d) X^+. (See Fig. 1.) The transitions of X^0 and XX^0 are polarized along $[110]$ and $[1\bar{1}0]$, and the degree of this polarization strongly depends on height. For X^- and X^+, the transitions are not polarized along $[110]$ or $[1\bar{1}0]$.

$$P_i(T;\chi^q) = \mathcal{N}\exp\{-[E^{(i)}(\chi^q) - E^{(0)}(\chi^q)]/k_BT\} \quad (16)$$

is the occupation (Boltzmann) probability of the initial state $|\Psi^{(i)}(\chi^q)\rangle$ at temperature T; $\mathcal{N}$ is a normalization constant such that $\Sigma_i P_i(T;\chi^q)=1$ and k_B is the Boltzmann constant. Then, as *in-plane* polarizations $\hat{\mathbf{e}}_1=[110]$ and $\hat{\mathbf{e}}_2=[1\bar{1}0]$ have been probed extensively, we introduce the in-plane polarization anisotropy parameter λ,

$$\lambda(\omega,T;\chi^q) = \frac{I^{([110])}(\omega,T;\chi^q) - I^{([1\bar{1}0])}(\omega,T;\chi^q)}{I^{([110])}(\omega,T;\chi^q) + I^{([1\bar{1}0])}(\omega,T;\chi^q)}. \quad (17)$$

Thus, $\lambda=1$ indicates an optical transition that is *fully* polarized along the $[110]$ direction, while $\lambda=-1$ indicates one *fully* polarized along $[1\bar{1}0]$.

A. In-plane polarization anisotropy of the lowest optical transitions of X^0, X^-, X^+, and XX^0

Figure 4 shows the in-plane polarization anisotropy λ for the lowest optical transitions of (a) X^0, (b) XX^0, (c) X^-, and (d) X^+ as a function of dot height. Two features are prominent:

(i) The bright transitions $\omega_{20}(X^0)$ and $\omega_{30}(X^0)$ are polarized and the polarization anisotropy depends on height; see Fig. 4(a). Similarly, the lowest transitions of the biexciton $\omega_{03}(XX^0)$ and $\omega_{02}(XX^0)$ are polarized and the degree of polarization also depends on height. These transitions correspond to the *decay* into the two bright states of the monoexciton [Fig. 1(d)]. Clearly, the biexciton transitions inherit the polarization of the monoexciton transitions. For both X^0 and XX^0, we see that λ switches sign as a function of height. In particular, at $h=50$ Å the transitions of X^0 present no in-plane polarization anisotropy [see arrow in Figs. 4(a)] because the bright doublet formed by $|\Psi^{(2)}(X^0)\rangle$ and $|\Psi^{(3)}\times(X^0)\rangle$ is degenerate, which according to our calculation results in $I^{([110])}(\omega_{20}) \simeq I^{([1\bar{1}0])}(\omega_{20})$.

(ii) The lowest optical transitions of X^- and X^+ have degenerate transition (recombination) energies [Fig. 1(c) and 1(d)] and, according to our calculations, this results in $I^{([110])}(\omega_{00}) \simeq I^{([1\bar{1}0])}(\omega_{00})$ and, thus, negligible in-plane polarization anisotropy regardless of height.

In addition to (i) and (ii), we find that (iii) the in-plane polarization anisotropy of the lowest transitions of X^0 and XX^0 depends dramatically on the dot's alloy randomness (disorder realization); as shown in Fig. 5 for seven alloy realizations in a 35 Å-tall dot. For a given transition in both X^0 and XX^0, λ switches sign depending on alloy randomness. Further, while some alloy realizations like 4 and 5 result in transitions nearly fully polarized ($\lambda \sim 99\%$), others such as 2, 6 and 7 present small anisotropy ($\lambda \sim 20\%$).

IV. RADIATIVE RECOMBINATION LIFETIMES

The *characteristic* radiative lifetime $\tau_{if}(\chi^q)$ of a transition $|\Psi^{(i)}(\chi^q)\rangle \rightarrow |\Psi^{(f)}(\chi^q - 1)\rangle$ follows from both the magnitude of the dipole matrix element of the transition $|\mathrm{M}_{if}^{(\hat{\mathbf{e}})}(\chi^q)|^2$ and the recombination energy ω_{if}.[27] Namely,

$$\frac{1}{\tau_{if}(\chi^q)} = \frac{4}{3}\left(\frac{e^2}{m_0^2c^3\hbar^2}\right) n\omega_{if}(\chi^q) \sum_{\hat{\mathbf{e}}=\hat{x},\hat{y},\hat{z}} |\mathrm{M}_{if}^{(\hat{\mathbf{e}})}(\chi^q)|^2. \quad (18)$$

Here, e and m_0 are the charge and mass of the electron, respectively, and c is the velocity of light in vacuum. In addition, the refractive index n of the dot material accounts for the material's effects on the photon emission. The linear dependence of $1/\tau_{if}(\chi^q)$ on refractive index is applicable only when considering dot and matrix materials with similar dielectric constants, as it is the case in (In,Ga)As/GaAs dots. In a more general case, more complicate dependences have been proposed.[28] Note that the characteristic radiative lifetime [Eq. (18)] does not depend on temperature nor on the occupation probability of the initial state $|\Psi^{(i)}(\chi^q)\rangle$, as it

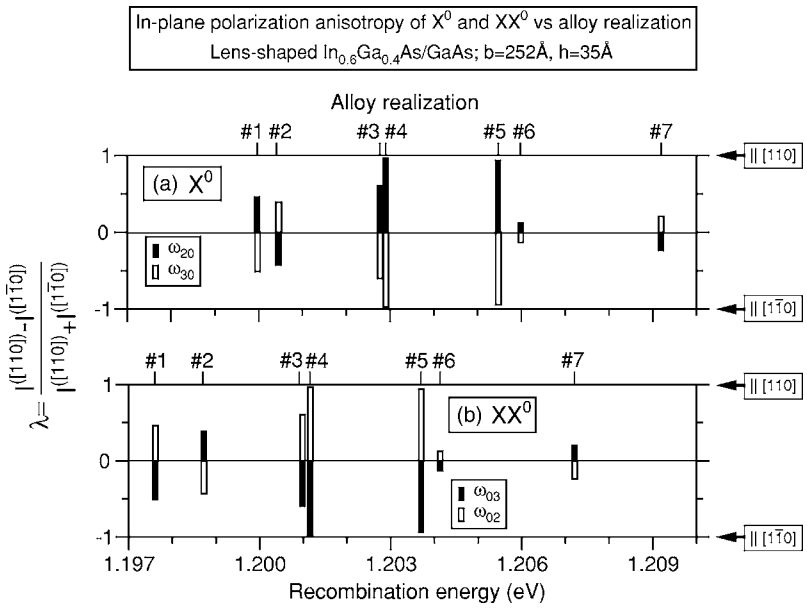

FIG. 5. In-plane polarization λ for the lowest optical transitions of (a) X^0 and (b) XX^0 for different realizations of alloy randomness in a 35 Å tall $In_{0.6}Ga_{0.4}As/GaAs$ dot (base $b=252$ Å). For both X^0 and XX^0, λ depends dramatically on alloy realization, changing not only its sign but its magnitude too.

is a characteristic property of the transition $|\Psi^{(i)}(\chi^q)\rangle \rightarrow |\Psi^{(f)}(\chi^q-1)\rangle$. On the other hand, the actual radiative lifetime $\tau(\chi^q)$ of exciton χ^q depends both on the probability n_i of having the initial states $|\Psi^{(i)}(\chi^q)\rangle$ of exciton χ^q occupied and the number of final states $|\Psi^{(f)}(\chi^q-1)\rangle$ of exciton χ^q-1 available for recombination, as well as on the characteristic radiative lifetimes $\tau_{if}(\chi^q)$. We calculate $\tau(\chi^q)$ from

$$\frac{1}{\tau(\chi^q)} = \sum_f \sum_i n_i \frac{1}{\tau_{if}(\chi^q)}. \tag{19}$$

Here, $\Sigma_i n_i = 1$ and $n_i = n_i(T;\chi^q)$ where T is the temperature of the system. In general, the calculation of n_i involves solving a system of rate equations.[29] However, in the case that the intra-level relaxation of exciton χ^q is much faster than the radiative lifetimes, n_i is given by the Boltzmann weight $P_i(T;\chi^q)$ [Eq. (16)].

A. Radiative lifetime $\tau(\chi^q)$ of the lowest optical transitions of X^0, X^-, X^+, and XX^0

Monoexciton. At $T=0$ K, and assuming fast non-radiative relaxation to the dark ground-state of X^0, the radiative lifetime of the monoexciton $\tau(X^0)$ equals the characteristic radiative lifetime $\tau_{00}(X^0)$ and it is long (~ ms). At finite temperatures, all four levels [Fig. 1(a)] of the X^0 ground state are thermally populated and emit light with their own characteristic lifetime [Eq. (18)]. For temperatures such that the lowest four monoexciton states are occupied, while the occupation of excited states is negligible, we calculate the radiative lifetime from Eq. (19) and find

$$\tau(X^0) = 4\left[\frac{\tau_{20}(X^0)\tau_{30}(X^0)}{\tau_{20}(X^0)+\tau_{30}(X^0)}\right] \simeq 2\tau_{20}(X^0). \tag{20}$$

Here, we have used a result of our calculations that predict $\tau_{20}(X^0) \simeq \tau_{30}(X^0)$ regardless of dot height. In addition, we have neglected the long-lived recombinations ω_{00} and ω_{10}. Figure 6(a) shows the characteristic $\tau_{20}(X^0)$ versus dot height. We find that this lifetime depends weakly on height. A calculation of $\tau(X^0)$ at $T=10$ K predicts a moderate decrease in the monoexciton radiative lifetime as height increases [Fig. 6(b)]. It should be noted that $\tau(X^0)$ is actually bigger than the approximate value of $2\tau_{20}(X^0)$ [Eq. (20)] due to the actual occupation probability $n_i(10\text{ K}, X^0)$ of the initial states. By measuring time-resolved photoluminescence in InAs/GaAs dots ($b=120-220$ Å, height unspecified) with monoexciton emission ranging from 1.2–1.3 eV, Karachinsky and co-workers have recently observed the opposite trend,[30] i.e., $\tau(X^0)$ increases with dot size from 1 ns in a dot with emission energy of 1.31 eV to ~3 ns in one with emission energy of 1.25 eV. The values of $\tau(X^0)$ we predict for tall dots ($h=65$ Å and 75 Å) agree satisfactorily with the value of 1 ns measured by Buckle *et al.* for an InAs/GaAs dot ($b\sim 120$ Å, $h\sim 30$ Å) with gap 1.131 eV (Ref. 31) at a temperature of 6 K. Further, our predictions also agree well with the value of 1.55 ns extracted from time-resolved photoluminescence experiments at 10 K performed in InAs/GaAs dots ($b=200$ Å, $h=20$ Å) by Bardot and co-workers.[32]

Biexciton. In contrast to the monoexciton, the biexciton ground state is singly-degenerate and bright [Fig. 1(b)]. Thus, at $T=0$ K, the radiative lifetime is given from Eq. (19) as

$$\tau(XX^0) = \left[\frac{\tau_{02}(XX^0)\tau_{03}(XX^0)}{\tau_{02}(XX^0)+\tau_{03}(XX^0)}\right] \simeq \frac{1}{2}\tau_{03}(XX^0). \tag{21}$$

Similarly to the X^0 case, in Eq. (21) we have used the relationship $\tau_{03}(XX^0) \simeq \tau_{02}(XX^0)$ that our calculations predict, and we have neglected the long-lived dark recombination channels. Figure 6(a) shows $\tau_{03}(XX^0)$ as a function of height. We find a weak dependence with height, as in the monoexciton case. Remarkably, we find that $\tau_{20}(X^0) \simeq \tau_{03}(XX^0)$ regardless of height. The latter leads to the following relationship between the radiative lifetime of the monoexciton and biexciton,

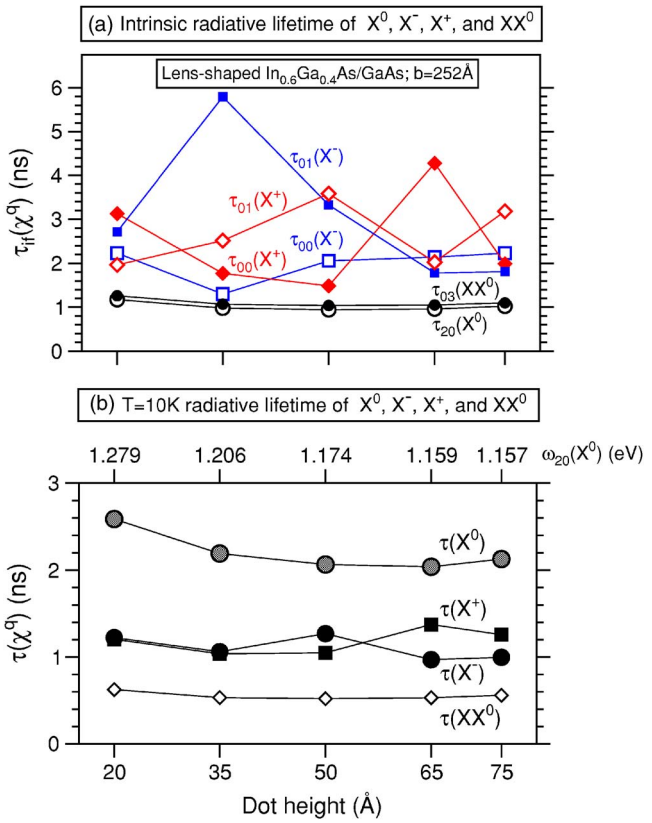

FIG. 6. (Color online) (a) Characteristic radiative lifetime $\tau_{if}(\chi^q)$ [Eq. (18)] of the lowest optical transition of X^0, X^-, X^+, and XX^0 as a function of dot height. For X^0 and XX^0, the characteristic lifetimes are nearly the same and depend weakly on height. A stronger dependence on height is found for X^- and X^+. (b) $T=10$ K radiative lifetime $\tau(\chi^q)$ [Eq. (19)] of the lowest optical transition of X^0, X^-, X^+, and XX^0 as a function of dot height. The lifetimes depend weakly on height for all these excitons. For X^0 and XX^0, the lifetimes are nearly the same. A similar trend is found for X^- and X^+. At all heights, the radiative lifetimes of X^- and X^+ are about twice as big as that of XX^0.

$$\tau(XX^0) \simeq \frac{1}{4}\tau(X^0). \tag{22}$$

Figure 6(b) shows that at $T=10$ K the calculated $\tau(XX^0)$ depends weakly on height, changing by about 0.1 ns in the entire range of heights studied. $\tau(XX^0)$ is in excellent agreement with the value of 0.5 ns measured by Ulrich *et al.* in an (In,Ga)As/GaAs quantum dot ($b=150-200$ Å, $h=10-20$ Å) with an exciton gap of 1.337 eV (Ref. 33).

Trions. Both X^- and X^+ have a two-fold degenerate ground state that is bright [Figs. 1(c) and 1(d)]. In each of these excitons, there are four lowest transitions; namely, $\omega_{00}(X^-)$ [Fig. 1(c)], $\omega_{10}(X^-)$, $\omega_{01}(X^-)$, and $\omega_{11}(X^-)$; and $\omega_{00}(X^+)$ [Fig. 1(d)], $\omega_{10}(X^+)$, $\omega_{01}(X^+)$, and $\omega_{11}(X^+)$, for X^- and X^+, respectively. In turn, each of these transitions have a corresponding characteristic radiative lifetime. For the latter, our calculations predict $\tau_{00}(X^-)=\tau_{11}(X^-)$ and $\tau_{01}(X^-)=\tau_{10}(X^-)$ as well as $\tau_{00}(X^+)=\tau_{11}(X^+)$ and $\tau_{01}(X^+)=\tau_{10}(X^+)$. Thus, at $T=0$ K, the radiative lifetimes of X^- and X^+ are given by

$$\tau(X^-) = \left\{\frac{1}{2}\left[\frac{1}{\tau_{00}(X^-)}+\frac{1}{\tau_{01}(X^-)}\right]+\frac{1}{2}\left[\frac{1}{\tau_{10}(X^-)}+\frac{1}{\tau_{11}(X^-)}\right]\right\}^{-1} = \frac{\tau_{00}(X^-)\tau_{01}(X^-)}{\tau_{00}(X^-)+\tau_{01}(X^-)}, \tag{23}$$

$$\tau(X^+) = \left\{\frac{1}{2}\left[\frac{1}{\tau_{00}(X^+)}+\frac{1}{\tau_{01}(X^+)}\right]+\frac{1}{2}\left[\frac{1}{\tau_{10}(X^+)}+\frac{1}{\tau_{11}(X^+)}\right]\right\}^{-1} = \frac{\tau_{00}(X^+)\tau_{01}(X^+)}{\tau_{00}(X^+)+\tau_{01}(X^+)}. \tag{24}$$

Figure 6(a) shows the height dependence of $\tau_{00}(X^-)$ and $\tau_{01}(X^-)$, and $\tau_{00}(X^+)$ and $\tau_{01}(X^+)$. These *characteristic* radiative lifetimes depend strongly and non-monotonically on height. This nonmonotonic dependence translates into a rather simple and monotonic $\tau(X^-)$ and $\tau(X^+)$, as shown in Fig. 6(b). For flat dots $\tau(X^-)\simeq\tau(X^+)$, whereas for taller dots these lifetimes become slightly different. Our predicted $\tau(X^-)$ are in satisfactory agreement with the value of 0.6 ns recently observed by Smith and co-workers in $In_xGa_{1-x}As/GaAs$ dots (size unspecified) with exciton ground-state emission at ~1.318 eV (Ref. 1). We find that the radiative lifetimes of the charged trions satisfy the relationship $\tau(X^0)>\tau(X^-)\sim\tau(X^+)>\tau(XX^0)$.

V. COMPARISON OF X^0, X^-, X^+, AND XX^0 IN LENS-SHAPED PURE InAs/GaAs WITH ALLOYED (In,Ga)As/GaAs DOTS

For completeness, we briefly compare the binding and recombination energies, polarization anisotropy, and radiative lifetimes in lens-shaped pure, nonalloyed InAs/GaAs dots with $In_{0.6}Ga_{0.4}As/GaAs$ dots. Note that Williamson, Wang, and Zunger have already compared results for X^0 for several alloy profiles.[16] In Ref. 25 we predicted that hole localization takes place at the dot-GaAs matrix interface as the height of these dots increases above 35 Å. Thus, we discuss here two flat dots ($h=20$ Å and 35 Å) with base $b=252$ Å.

(i) Recombination energies are smaller in InAs/GaAs dots than in $In_{0.6}Ga_{0.4}As/GaAs$ dots with the same geometry. For instance, $\omega_{20}(X^0)=1.078$ eV and 0.987 eV for $h=20$ Å and 35 Å, respectively.

(ii) The spectroscopic shifts show the same trends with height in flat InAs/GaAs as those in flat $In_{0.6}Ga_{0.4}As/GaAs$ dots. So do the binding energies $\Delta(X^-)$ and $\Delta(X^+)$, and $\Delta(XX^0)$. However, there are two important differences between the pure, non-alloyed InAs/GaAs dots and their $In_{0.6}Ga_{0.4}As/GaAs$ counterparts: (a) For the 20 Å-tall InAs/GaAs dot, while the binding energies still satisfy $\Delta(X^-)>\Delta(XX^0)>\Delta(X^+)$, we find that both X^+ and XX^0 are *bound*, with $\Delta(X^+)=1.6$ meV and $\Delta(XX^0)=1.5$ meV, respectively. This is so because at this height the InAs/GaAs dot is in the nearly "symmetric" regime: $J_{00}^{(hh)}=25.6$ meV $\sim J_{00}^{(ee)}=25.1$ meV $\sim J_{00}^{(eh)}=25.3$ meV, so the Hartree-Fock component of the binding energy [see Eq. (13) for XX^0 case] is much smaller than in the $In_{0.6}Ga_{0.4}As/GaAs$ dot with same

height. Thus, correlation becomes capable of binding X^+ and XX^0 in the pure, nonalloyed dot. (b) For the 35 Å-tall InAs/GaAs dot, we find *ordering reversal*, i.e. $\Delta(X^+) > \Delta(XX^0) > \Delta(X^-)$. In $In_{0.6}Ga_{0.4}As/GaAs$ dots, this ordering is attained at $h=50$ Å (Fig. 3).

(iii) In contrast to the findings in $In_{0.6}Ga_{0.4}As/GaAs$ dots, transitions $\omega_{20}(X^0)$ and $\omega_{30}(X^0)$ are fully polarized along $[110]$ ($\lambda=1$) and $[1\bar{1}0]$ ($\lambda=-1$), respectively, regardless of height. Consequently, $\omega_{03}(XX^0)$ and $\omega_{02}(XX^0)$ are fully polarized along $[1\bar{1}0]$ and $[110]$, respectively. These polarizations are indeed expected from a dot with C_{2v} symmetry, like a lens-shaped pure InAs/GaAs dot.

(iv) Radiative lifetimes $\tau(X^0)$, $\tau(X^+)$ and $\tau(X^-)$, and $\tau(XX^0)$ are similar to those in $In_{0.6}Ga_{0.4}As/GaAs$ dots with the same geometry. For instance, $\tau(X^0)=2.8$ ns and $\tau(XX^0)=0.7$ ns for $h=35$ Å; and $\tau(X^0)=2.9$ ns and $\tau(XX^0)=0.6$ ns for $h=20$ Å.

VI. SUMMARY

We have addressed the height dependence of recombination energies, polarization and radiative lifetimes of the lowest optical transitions of the neutral exciton (X^0), negatively (X^-) and positively charged (X^+) trions, and the biexciton (XX^0) in lens-shaped, self assembled $In_{0.6}Ga_{0.4}As/GaAs$ quantum dots. We have predicted the following.

(i) The recombination energy of the lowest transition of X^-, X^+ and XX^0, correspondingly, $\omega_{00}(X^-)$, $\omega_{00}(X^+)$ and $\omega_{03}(XX^0)$ shows qualitatively different behavior for each excitonic complex. Namely, $\omega_{00}(X^-)$ blue-shifts as height increases, whereas that of $\omega_{00}(X^+)$ red-shifts. On the other hand, as height increases, $\omega_{03}(XX^0)$ shows a red-shift at small heights, reaches a maximum shift, and then blue-shifts for taller dots. This behavior is explained by the height dependence and relative magnitude of $J_{00}^{(ee)}$, $J_{00}^{(hh)}$ and $J_{00}^{(eh)}$.

(ii) The binding energies $\Delta(X^-)$, $\Delta(X^+)$ and $\Delta(XX^0)$ follow the height dependence of the emission spectroscopic shifts. Changes in the dot height drives a bound-to-unbound crossover for each of these complexes.

(iii) The in-plane polarization anisotropy λ of the lowest transitions of X^0 (ω_{20}) and XX^0 (ω_{03}) strongly depends on dot height as well as on alloy randomness (disorder realization). In contrast, the lowest transitions of X^- and X^+ present negligible λ regardless of height.

(iv) The ground state of X^0 encompasses four states that split off in a low-energy pair that is dark and a high-energy pair that is bright, with a bright-dark splitting that increases as height decreases. Thus, at $T=0$ K the radiative lifetime $\tau(X^0)$ of X^0 is long. On the other hand, at $T=10$ K both dark and bright states are populated; so, $\tau(X^0)$ becomes fast, moderately decreases as height increases, and its magnitude ranges from 2–3 ns. In contrast, $\tau(X^-)$, $\tau(X^+)$ and $\tau(XX^0)$ are fast even at $T=0$ K, as a consequence of these excitons having ground states that are bright. These radiative lifetimes depend weakly on height. Further, $\tau(X^-) \sim \tau(X^+) \simeq 1.1$ ns, while $\tau(XX^0) \simeq 0.5$ ns.

We have compared these predictions with available data and have found them in satisfactory agreement. In addition, we compared with results in pure, nonalloyed InGa/GaAs quantum dots.

ACKNOWLEDGMENTS

We thank Alberto Franceschetti (NREL) for valuable discussions. This work has been supported by U.S. DOE-SC-BES-DMS under Contract No. DE-AC36-99GO10337.

[1] J. M. Smith, P. A. Dalgarno, R. J. Warburton, A. O. Govorov, K. Karrai, B. D. Gerardot, and P. M. Petroff, Phys. Rev. Lett. **94**, 197402 (2005).

[2] M. E. Ware, A. S. Bracker, E. Stinaff, D. Gammon, D. Gershoni, and V. L. Korenev, Physica E (Amsterdam) **26**, 55 (2005).

[3] M. S. Skolnick and D. J. Mowbray, Annu. Rev. Mater. Res. **34**, 181 (2004).

[4] F. Guffarth, S. Rodt, A. Schliwa, K. Pötschke, and D. Bimberg, Physica E (Amsterdam) **25**, 261 (2004).

[5] J. J. Finley, A. D. Ashmore, A. Lemaître, D. J. Mowbray, M. S. Skolnick, I. E. Itskevich, P. A. Maksym, M. Hopkinson, and T. F. Krauss, Phys. Rev. B **63**, 073307 (2001).

[6] S. Rodt, R. Heitz, R. L. Sellin, A. Schliwa, K. Pötschke, and D. Bimberg, Physica E (Amsterdam) **21**, 1065 (2004); S. Rodt, R. Heitz, A. Schliwa, R. L. Sellin, F. Guffarth, and D. Bimberg, Phys. Rev. B **68**, 035331 (2003).

[7] B. Urbaszek, R. J. Warburton, K. Karrai, B. D. Gerardot, P. M. Petroff, and J. M. Garcia, Phys. Rev. Lett. **90**, 247403 (2003).

[8] F. Findeis, A. Zrenner, G. Böhm, and G. Abstreiter, Solid State Commun. **114**, 227 (2000).

[9] L. Landin, M. S. Miller, M.-E. Pistol, C. E. Pryor, and L. Samuelson, Science **280**, 262 (1998); L. Landin, M.-E. Pistol, C. Pryor, M. Persson, L. Samuelson, and M. Miller, Phys. Rev. B **60**, 16640 (1999).

[10] D. Bimberg, M. Grundmann, and N. N. Ledenstov, *Quantum Dot Heterostructures* (Wiley, Chichester, 1999); C. Delerue and M. Lannoo, *Nanostructures—Theory and Modeling* (Springer-Verlag, Berlin, 2004); T. Takagahara, Phase Transitions **68**, 281 (1999); U. Woggon, *Optical Properties of Semiconductor Quantum Dots* (Springer-Verlag, Berlin, 1997).

[11] L.-W. Wang and A. Zunger, Phys. Rev. B **59**, 15806 (1999).

[12] L. W. Wang, A. J. Williamson, A. Zunger, H. Jiang, and J. Singh, Appl. Phys. Lett. **76**, 339 (2000).

[13] A. Zunger, Phys. Status Solidi B **224**, 727 (2001).

[14] S. Lee, O. L. Lazarenkova, P. von Allmen, F. Oyafuso, and G. Klimeck, Phys. Rev. B **70**, 125307 (2004); S. Lee, F. Oyafuso, P. von Allmen, and G. Klimeck, Phys. Rev. B **69**, 045316 (2004); R. Santoprete, B. Koiller, R. B. Capaz, P. Kratzer, Q. K. K. Liu, and M. Scheffler, Phys. Rev. B **68**, 235311 (2003).

[15] W. Sheng, S.-J. Cheng, and P. Hawrylak, Phys. Rev. B **71**, 035316 (2005).

[16] A. J. Williamson, L.-W. Wang, and A. Zunger, Phys. Rev. B **62**,

12963 (2000).
[17] A. Franceschetti, H. Fu, L. W. Wang, and A. Zunger, Phys. Rev. B **60**, 1819 (1999).
[18] R. Resta, Phys. Rev. B **16**, 2717 (1977).
[19] G. Bester, S. Nair, and A. Zunger, Phys. Rev. B **67**, 161306(R) (2003).
[20] M. Bayer, G. Ortner, O. Stern, A. Kuther, A. A. Gorbunov, A. Forchel, P. Hawrylak, S. Fafard, K. Hinzer, T. L. Reinecke, S. N. Walck, J. P. Reithmaier, F. Klopf, and F. Schäfer, Phys. Rev. B **65**, 195315 (2002).
[21] P. Y. Yu and M. Cardona, *Fundamentals of Semiconductors—Physics and Materials Properties* (Springer, Berlin, 2001).
[22] G. Bester and A. Zunger, Phys. Rev. B **68**, 073309 (2003).
[23] J. Shumway, A. Franceschetti, and A. Zunger, Phys. Rev. B **63**, 155316 (2001).
[24] G. A. Narvaez, G. Bester, and A. Zunger, Phys. Rev. B **72**, 041307(R) (2005).
[25] G. A. Narvaez, G. Bester, and A. Zunger, J. Appl. Phys. **98**, 043708 (2005).
[26] M. Bayer, T. Gutbrod, A. Forchel, V. D. Kulakovskii, A. Gorbunov, M. Michel, R. Steffen, and K. H. Wang, Phys. Rev. B **58**, 4740 (1998).
[27] D. L. Dexter, *Solid State Physics* (Academic Press, New York, 1958), Vol. 6.
[28] A. Thränhardt, C. Ell, G. Khitrova, and H. M. Gibbs, Phys. Rev. B **65**, 035327 (2002).
[29] E. Dekel, D. Regelman, D. Gershoni, E. Ehrenfreund, W. V. Schoenfeld, and P. M. Petroff, Phys. Rev. B **62**, 11038 (2000).
[30] L. Ya. Karachinsky, S. Pellegrini, G. A. Buller, A. S. Sholnik, N. Yu. Gordeev, V. P. Evtikhiev, and V. B. Novikov, Appl. Phys. Lett. **84**, 7 (2004).
[31] P. D. Buckle, P. Dawson, S. A. Hall, X. Chen, M. J. Steer, D. J. Mowbray, M. S. Skolnick, and M. Hopkinson, J. Appl. Phys. **86**, 2555 (1999).
[32] C. Bardot, M. Schwab, M. Bayer, S. Fafard, Z. Wasilewski, and P. Hawrylak, Phys. Rev. B **72**, 035314 (2005).
[33] S. M. Ulrich, M. Benyoucef, P. Michler, N. Baer, P. Gartner, F. Jahnke, M. Schwab, H. Kurtze, M. Bayer, S. Fafard, Z. Wasilewski, and A. Forchel, Phys. Rev. B **71**, 235328 (2005).